eLIFE
elifesciences.org

# Figures and figure supplements

Noise-induced plasticity of KCNQ2/3 and HCN channels underlies vulnerability and resilience to tinnitus

**Shuang Li, et al.**

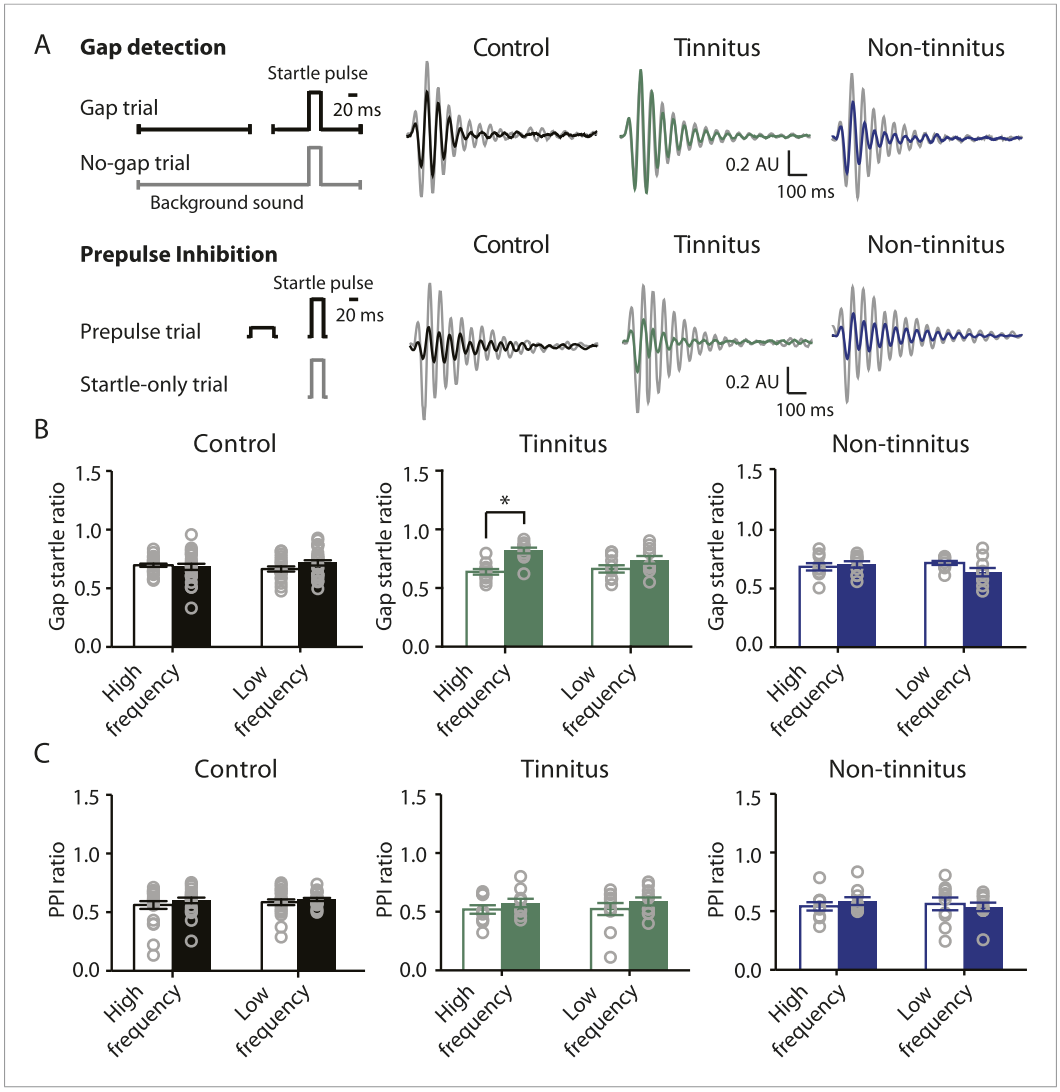


**Figure 1**. Mouse model of tinnitus allows for behavioral separation of noise-exposed mice with either vulnerability or resilience to tinnitus. **A**. Top left: diagram illustrating gap and no-gap trials in the gap detection behavioral assay. Top right: representative startle responses in no-gap (always in gray) and gap trials from control (black), tinnitus (green), and non-tinnitus (blue) mice. AU: Arbitrary unit. Bottom left: diagram illustrating startle-only and prepulse trials in the prepulse inhibition (PPI) behavioral assay. Bottom right: representative startle responses in startle-only (always in gray) and prepulse trials from control (black), tinnitus (green), and non-tinnitus (blue) mice. **B**. Summary graphs of gap startle ratio (response to gap trial/response to no-gap trial) before (open bar) and 1 week after noise exposure (filled bar) for high- and low-frequency background sounds (high-frequency background, 20–32 kHz, control: n = 21, p = 0.6; tinnitus: n = 11, p < 0.001; non-tinnitus: n = 10, p = 0.6; low frequency background, 10–16 kHz, control: n = 21, p = 0.42; tinnitus: n = 11, p = 0.06; non-tinnitus: n = 10, p = 0.07). **C**. Summary graphs of prepulse inhibition ratio (PPI ratio, response to prepulse trial/response to startle-only trial) before (open bar) and 1 week after noise exposure (filled bar) for high- and low-frequency prepulse (high-frequency background, 20–32 kHz, control: n = 21, p = 0.25; tinnitus: n = 11, p = 0.18; non-tinnitus: n = 10, p = 0.36; low frequency background, 10–16 kHz, control: n = 22, p = 0.56; tinnitus: n = 11, p = 0.17; non-tinnitus: n = 10, p = 0.56). Asterisk, p < 0.05. Error bars indicate SEM. See end of the manuscript for detailed values in **B** and **C**.

DOI: 10.7554/eLife.07242.003

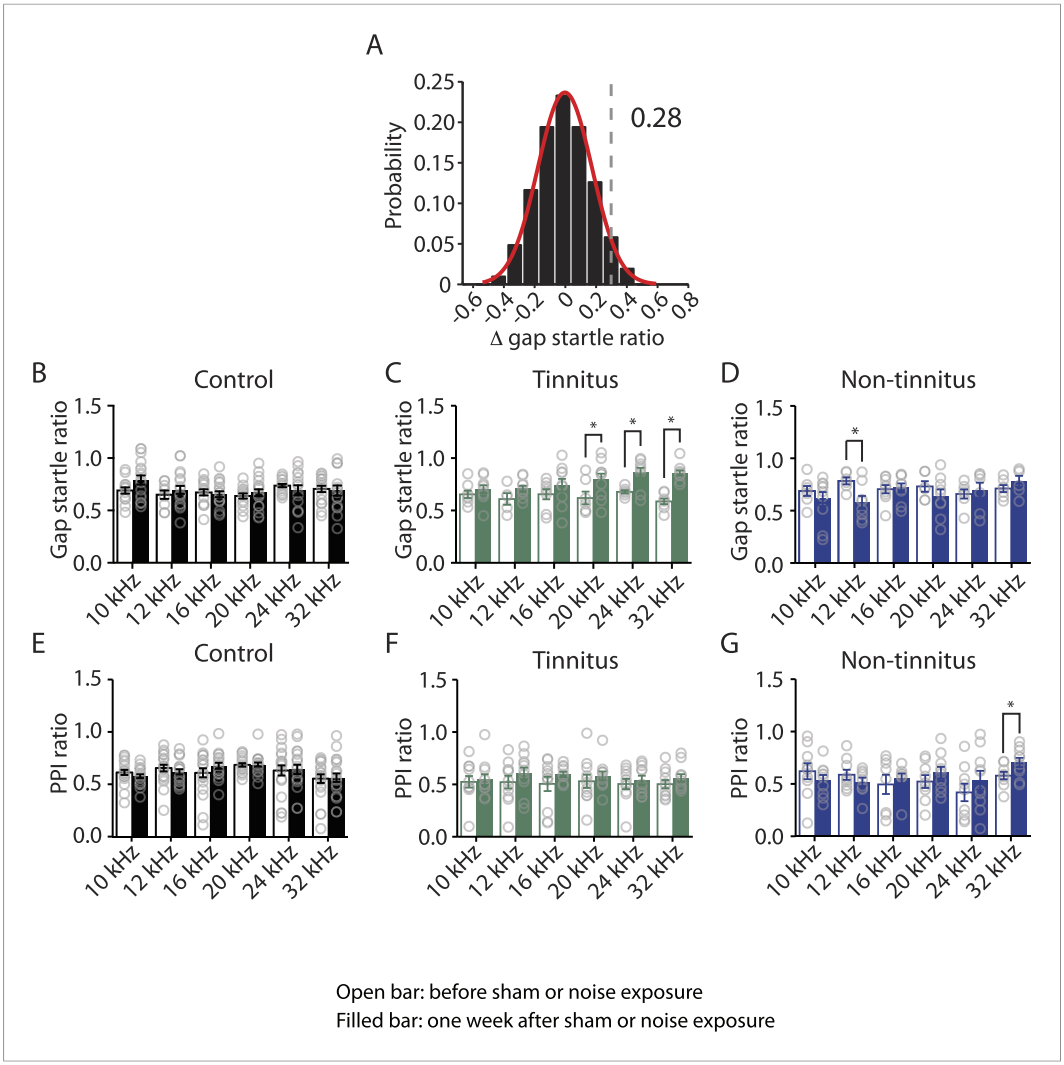


**Figure 1—figure supplement 1**. Tinnitus behavior (gap detection deficit) is detected with high-frequency background sounds. **A**. Probability distribution of changes in gap startle ratio (Δ gap startle ratio) in sham-exposed (control) mice. Δ gap startle ratio represents changes in control mice between postnatal day P17- P20 and P24 - P27. Data were fitted by a normal distribution (red curve, $\mu = -0.02$, $\delta = 0.15$, n = 21). Δ gap startle ratios smaller than 0.28 (dotted line), which is the point that is 2 standard deviations above the mean and is used as the threshold for evaluating tinnitus, represent 98.6% of the experimental Δ gap startle ratios and 98.5% of the fitted distribution. **B**. Summary graph of gap startle ratio for different frequencies of background for control mice: 10 kHz, before: 0.69 ± 0.03, n = 13, after: 0.79 ± 0.04, n = 17, p = 0.08; 12 kHz, before: 0.65 ± 0.04, n = 8, after: 0.70 ± 0.04, n = 18, p = 0.47; 16 kHz, before: 0.67 ± 0.03, n = 15, after: 0.66 ± 0.03, n = 18, p = 0.67; 20 kHz, before: 0.64 ± 0.02, n = 14, after: 0.67 ± 0.03, n = 18, p = 0.47; 24 kHz, before: 0.74 ± 0.02, n = 17, after: 0.69 ± 0.05, n = 14, p = 0.34; 32 kHz, before: 0.71 ± 0.03, n = 19, after: 0.69 ± 0.05, n = 16, p = 0.77. **C**. Summary graph of gap startle ratio for different frequencies of background for tinnitus mice: 10 kHz, before: 0.65 ± 0.04, n = 8, after: 0.70 ± 0.04, n = 10, p = 0.36; 12 kHz, before: 0.61 ± 0.06, n = 5, after: 0.71 ± 0.03, n = 10, p = 0.10; 16 kHz, before: 0.66 ± 0.05, n = 8, after: 0.74 ± 0.06, n = 10, p = 0.30; 20 kHz, before: 0.62 ± 0.06, n = 7, after: 0.80 ± 0.05, n = 11, p = 0.04; 24 kHz, before: 0.68 ± 0.02, n = 7, after: 0.86 ± 0.05, n = 9, p = 0.006; 32 kHz, before: 0.59 ± 0.03, n = 8, after: 0.86 ± 0.03, n = 12, p < 0.0001. **D**. Summary graph of gap startle ratio for different frequencies of background for non-tinnitus mice: 10 kHz, before: 0.69 ± 0.05, n = 7, after: 0.61 ± 0.07, n = 10, p = 0.40; 12 kHz, before: 0.78 ± 0.03, n = 6, after: 0.58 ± 0.06, n = 8, p = 0.02; 16 kHz, before: 0.71 ± 0.04, n = 6, after: 0.72 ± 0.04, n = 9, p = 0.83; 20 kHz, before: 0.73 ± 0.05, n = 6, after: 0.64 ± 0.06, n = 9, p = 0.32; 24 kHz, before: 0.66 ± 0.04, n = 7, after: 0.70 ± 0.07, n = 9, p = 0.67; 32 kHz, before: 0.71 ± 0.03, n = 7, after: 0.78 ± 0.05, n = 6, p = 0.26. **E**. Summary graph of PPI ratio for different frequencies of background sound for control mice: 10 kHz, before: 0.61 ± 0.02, n = 21, after: 0.58 ± 0.02, n = 21, p = 0.24; 12 kHz, before: 0.66 ± 0.03, n = 21, after: 0.62 ± 0.02, n = 21, p = 0.34; 16 kHz, before: 0.61 ± 0.04, n = 21, after: 0.68 ± 0.03, n = 19, p = 0.21; 20 kHz, before: 0.69 ± 0.02, n = 20, after: 0.69 ±

*Figure 1—figure supplement 1. continued on next page*

*Figure 1—figure supplement 1. Continued*

0.02, n = 21, p = 0.90; 24 kHz, before: 0.63 ± 0.05, n = 21, after: 0.64 ± 0.04, n = 19, p = 0.87; 32 kHz, before: 0.55 ± 0.04, n = 21, after: 0.56 ± 0.04, n = 21, p = 0.87. **F**. Summary graph of PPI ratio for different frequencies of background sound for tinnitus mice: 10 kHz, before: 0.52 ± 0.06, n = 11, after: 0.55 ± 0.05, n = 11, p = 0.79; 12 kHz, before: 0.52 ± 0.06, n = 11, after: 0.61 ± 0.05, n = 11, p = 0.32; 16 kHz, before: 0.51 ± 0.07, n = 11, after: 0.60 ± 0.03, n = 10, p = 0.24; 20 kHz, before: 0.53 ± 0.06, n = 11, after: 0.58 ± 0.04, n = 11, p = 0.51; 24 kHz, before: 0.50 ± 0.05, n = 11, after: 0.54 ± 0.04, n = 11, p = 0.56; 32 kHz, before: 0.50 ± 0.04, n = 11, after: 0.56 ± 0.04, n = 11, p = 0.28. **G**. Summary graph of PPI ratio for different frequencies of background sound for non-tinnitus mice: 10 kHz, before: 0.62 ± 0.08, n = 10, after: 0.54 ± 0.05, n = 10, p = 0.36; 12 kHz, before: 0.59 ± 0.05, n = 9, after: 0.52 ± 0.04, n = 9, p = 0.3; 16 kHz, before: 0.50 ± 0.09, n = 8, after: 0.55 ± 0.05, n = 9, p = 0.57; 20 kHz, before: 0.52 ± 0.06, n = 9, after: 0.61 ± 0.06, n = 10, p = 0.31; 24 kHz, before: 0.42 ± 0.08, n = 9, after: 0.54 ± 0.09, n = 10, p = 0.36; 32 kHz, before: 0.58 ± 0.04, n = 9, after: 0.71 ± 0.04, n = 10, p = 0.04. Asterisk, p < 0.05. Error bars indicate SEM.

DOI: 10.7554/eLife.07242.004

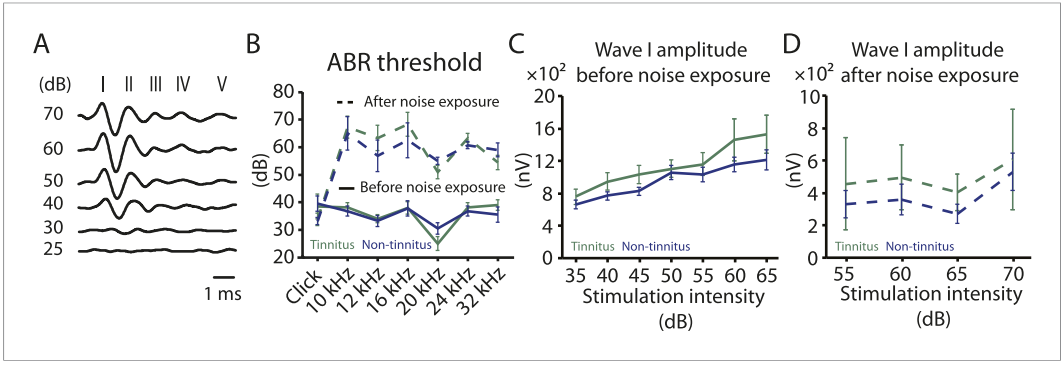


**Figure 2**. Tinnitus and non-tinnitus mice show similar ABR thresholds and suprathreshold ABR wave I amplitudes. **A**. Representative raw traces of auditory brainstem response (ABR) in response to click tone presented at different intensities (dB). I–V represent the different waves of the ABR. **B**. Summary graph of ABR thresholds for tinnitus (green) and non-tinnitus (blue) mice before (solid line) and 7 days (dashed line) after noise exposure (n = 5–11, no statistical difference was observed between tinnitus and non-tinnitus mice). **C**. Summary graph of suprathreshold wave I amplitudes for tinnitus (green) and non-tinnitus (blue) mice before noise exposure for high frequency (20–32 kHz) sound stimulation (n = 12–25, no statistical difference was observed between tinnitus and non-tinnitus mice). **D**. Summary graph of suprathreshold wave I amplitudes for tinnitus (green) and non-tinnitus (blue) mice 7 days after noise exposure for high frequency (20–32 kHz) sound stimulation (n = 4–10, no statistical difference was observed between tinnitus and non-tinnitus mice). See end of the manuscript for detailed values for **B**–**D**. Error bars indicate SEM.

DOI: 10.7554/eLife.07242.005

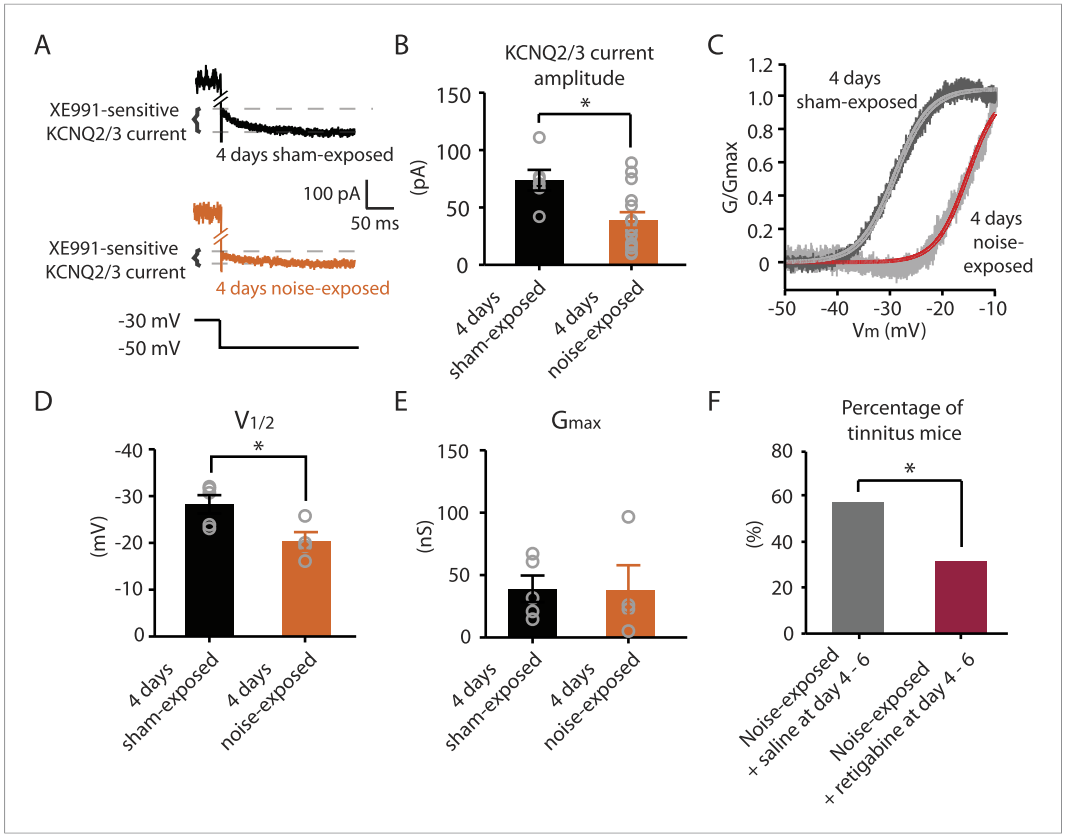


**Figure 3**. Noise-exposed mice show reduced KCNQ2/3 channel activity 4 days after noise exposure; this reduction is due to a depolarizing shift of $V_{1/2}$. **A**. Representative traces illustrating XE991 (10 μM)-sensitive KCNQ2/3 currents (Top) in fusiform cells from a 4 days sham-exposed (black) and a 4 days noise-exposed (yellow) mouse in response to a voltage step to –50 mV from a holding potential of –30 mV (Bottom; for clearer representation, currents were truncated along time axis). **B**. Summary graph showing KCNQ2/3 current amplitude in fusiform cells from 4 days sham-exposed and 4 days noise-exposed mice (4 days sham-exposed mice, 73.8 ± 9.05 pA, n = 6; 4 days noise-exposed mice, 39.16 ± 6.7 pA, n = 15, p = 0.01). **C**. Representative conductance–voltage relationship of XE991-sensitive current in 4 days sham-exposed (dark gray) and 4 days noise-exposed mice (light gray). Gray and red lines represent Boltzmann fits. **D**. Summary graph for Boltzmann fit parameter $V_{1/2}$ (4 days sham-exposed: –28.3 ± 1.9 mV, n = 5, 4 days noise-exposed: –20.3 ± 2.0 mV, n = 4, p = 0.03). **E**. Summary graph for Boltzmann fit parameter $G_{max}$ (4 days sham-exposed: 39.1 ± 10.2 nS, n = 5, 4 days noise-exposed: 37.7 ± 20.2 nS, n = 4, p = 0.90). **F**. Effect of retigabine injection 4–6 days after noise exposure on the percentage of mice that develop tinnitus. (Noise-exposed mice + saline at day 4–6: 57.1%, n = 14, noise-exposed mice + retigabine at day 4–6: 31.3%, n = 16, p = 0.03). Asterisk, p < 0.05. Error bars indicate SEM.

DOI: 10.7554/eLife.07242.006

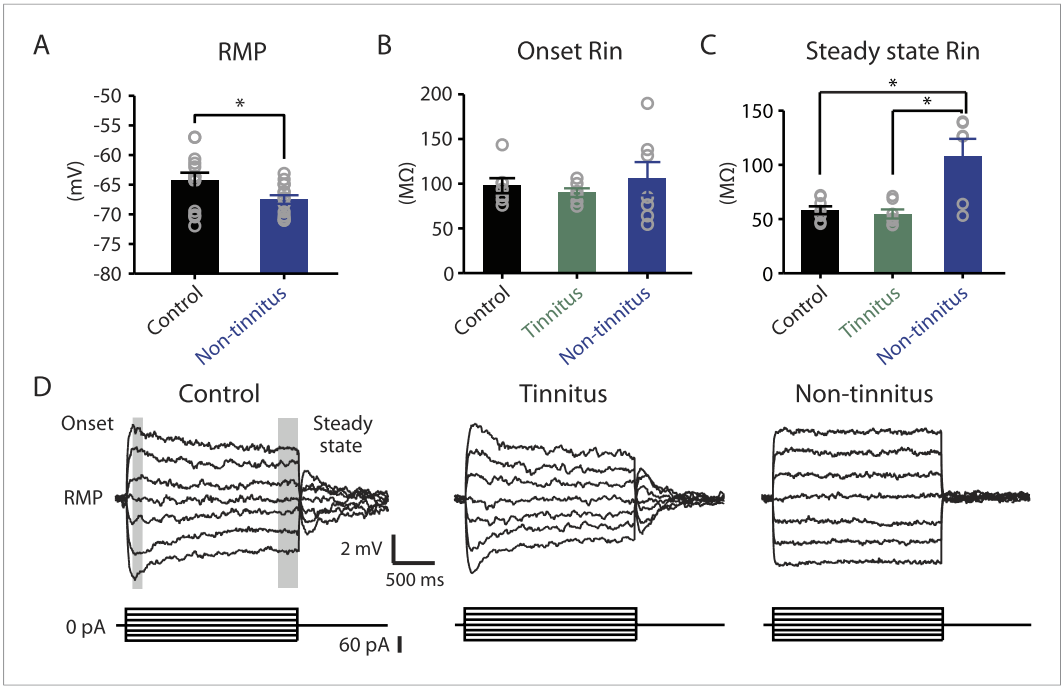


**Figure 4**. Non-tinnitus mice are biophysically distinct from control mice. **A**. Summary graph of resting membrane potential (RMP) of fusiform cells from control and non-tinnitus mice after blocking spontaneous firing with 0.5 μM TTX (control: –64.2 ± 1.3 mV, n = 14; non-tinnitus: –67.5 ± 0.7 mV, n = 15, p = 0.04). **B**. Summary graph of onset input resistance ($R_{in}$) of fusiform cells as measured in **D** from control, tinnitus and non-tinnitus mice (control: 97.9 ± 8.4 MΩ, n = 8; tinnitus: 90.1 ± 4.8 MΩ, n = 7; non-tinnitus: 105.7 ± 18.5 MΩ, n = 7, p = 0.73). **C**. Summary graph of steady-state $R_{in}$ of fusiform cells as measured in **D** from control, tinnitus, and non-tinnitus mice (control: 58.2 ± 3.6 MΩ, n = 8; tinnitus: 54.8 ± 4.2 MΩ, n = 7; non-tinnitus: 108.18 ± 15.9 MΩ, n = 7, p = 0.04). **D**. Representative voltage traces of fusiform cells from control, tinnitus, and non-tinnitus mice (Top) in response to small depolarizing and hyperpolarizing current steps (Bottom, –60 pA–60 pA, 20 pA step) for measuring input resistance. Shaded areas indicate the region for evaluating onset (starting from the peak of the voltage response, 100 ms width) and steady-state $R_{in}$ (starting at the voltage response 1.75 s after the current injection, 250 ms width). Asterisk, $p < 0.05$. Error bars indicate SEM.

DOI: 10.7554/eLife.07242.007

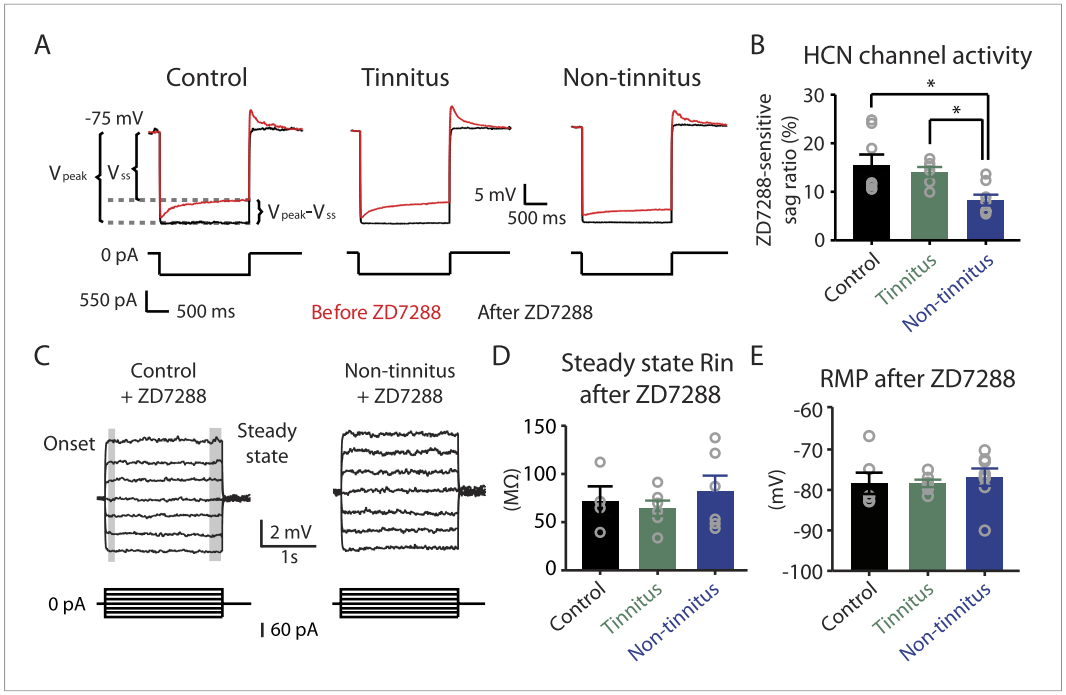


**Figure 5**. Reduced HCN channel activity in non-tinnitus mice underlies the biophysical differences between control and non-tinnitus mice. **A**. Representative voltage traces (Top) of fusiform cells from control, tinnitus, and non-tinnitus mice in response to a hyperpolarizing current step (Bottom) for measuring HCN channel activity before (red) and after (black) 10 μM ZD7288. HCN channel activity is measured by calculating the sag ratio ($V_{peak}$–$V_{ss}$)/$V_{peak}$*100 (%) that is sensitive to ZD7288. **B**. Summary graph showing HCN channel activity as measured by the protocol described in **A** (control: 15.5 ± 2.2%, n = 8; tinnitus: 14.1 ± 1.1%, n = 6; non-tinnitus: 8.3 ± 1.1%, n = 8, p = 0.02). **C**. Representative voltage traces of fusiform cells from control and non-tinnitus mice in response to current steps for measuring $R_{in}$ as in ***Figure 4D*** but now in the presence of 10 μM ZD7288. **D**. Summary graph showing steady-state $R_{in}$ in control, tinnitus, and non-tinnitus mice in 10 μM ZD7288 (control, 72.0 ± 15.1 MΩ, n = 4; tinnitus, 64.4 ± 8.0 MΩ, n = 6; non-tinnitus, 81.9 ± 16.4 MΩ, n = 6, p = 0.9). **E**. Summary graph showing resting membrane potential (RMP) in control, tinnitus, and non-tinnitus mice in 10 μM ZD7288 (control, −78.4 ± 2.6 mV, n = 6; tinnitus, −78.4 ± 0.9 mV, n = 6; non-tinnitus, −76.8 ± 2.1 mV, n = 8, p = 0.4). Asterisk, p < 0.05. Error bars indicate SEM.

DOI: 10.7554/eLife.07242.008

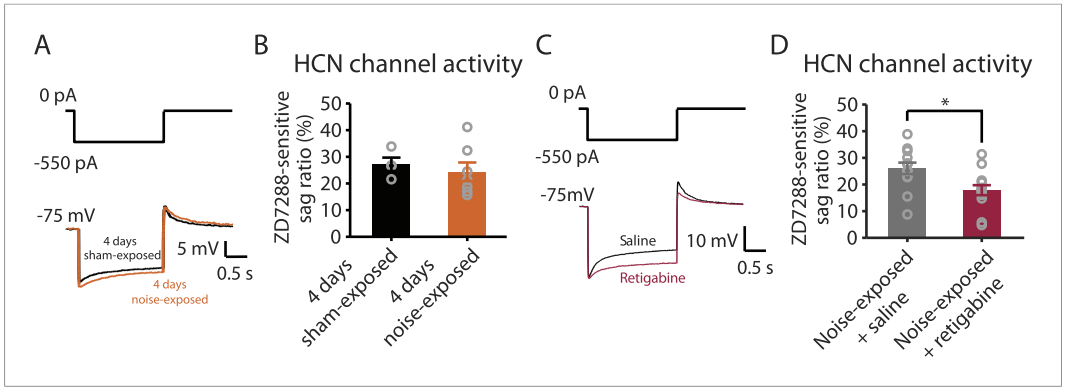


**Figure 6**. Noise-induced HCN plasticity occurs after KCNQ2/3 plasticity; KCNQ2/3 enhancement promotes HCN channel activity reduction. **A**. Representative voltage traces (Bottom) from fusiform cells in response to hyperpolarizing current step (Top) for measuring HCN channel activity in 4 days sham-exposed (black) and 4 days noise-exposed mice (yellow). **B**. Summary graph showing HCN channel activity in fusiform cells from 4 days sham-exposed and 4 days noise-exposed mice, measured as in ***Figure 5A,B*** (4 days sham-exposed mice, 27.2 ± 2.5%, n = 4; 4 days noise-exposed mice, 24.4 ± 3.5%, n = 7, p = 0.7). **C**. Representative voltage traces (Bottom) from fusiform cells in response to hyperpolarizing current step (top) for measuring HCN channel activity in noise-exposed with saline injection (black) and noise-exposed mice with retigabine injection (red). **D**. Summary graph showing HCN channel activity, as measured as in ***Figure 5A,B***. (Noise-exposed and saline-injected mice, 26.1 ± 0.6%, n = 13; noise-exposed retigabine-injected, 17.9 ± 0.5%, n = 14, p = 0.008). Asterisk, p < 0.05. Error bars indicate SEM.

DOI: 10.7554/eLife.07242.009

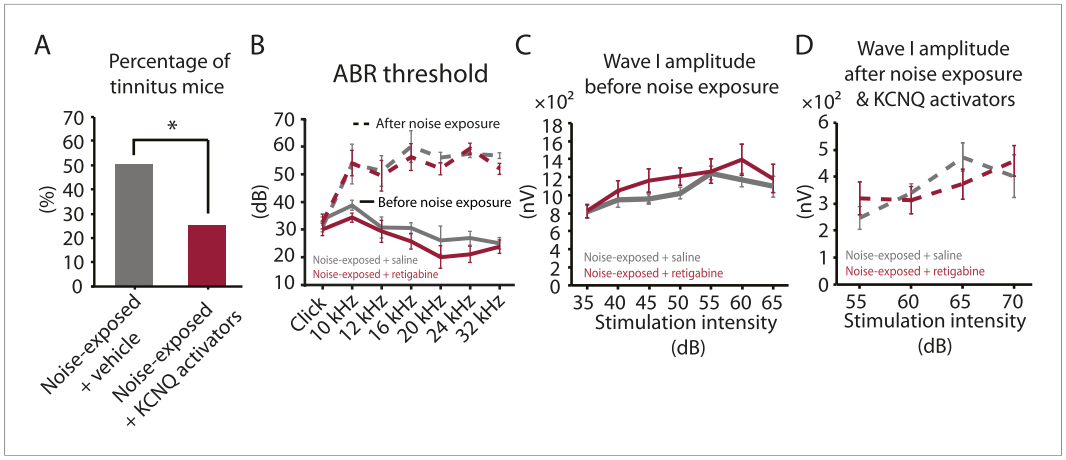


**Figure 7**. Injection of KCNQ activators after noise exposure reduces the incidence of tinnitus development without affecting threshold and suprathreshold ABRs. **A**. Percentage of mice that develop tinnitus (noise-exposed mice with intraperitoneal (IP) injection of vehicle, 50%, n = 18, noise-exposed mice with IP injection KCNQ channel activators, 25%, n = 20, p = 0.02). For noise-exposed mice with IP injection of vehicle (11 for retigabine vehicle and 7 flupirtine vehicle at 10 mg/kg); for noise-exposed mice with IP injection of KCNQ channel activators (10 for retigabine and 10 for flupirtine at 10 mg/kg). **B**. Summary graph of ABR thresholds from saline- (gray) and retigabine-injected (red) mice before (solid line) and 7 days after (dashed line) noise exposure and injection (n = 4–9, no statistical difference was observed between retigabine- and saline-injected mice). **C**. Summary graph of suprathreshold wave I amplitudes for noise-exposed mice + saline (gray) and noise-exposed mice + retigabine (red) before noise exposure for high frequency (20–32 kHz) sound stimulation (n = 5–15, no statistical difference was observed between retigabine- and saline-injected mice). **D**. Summary graph of suprathreshold wave I amplitudes for noise-exposed mice + saline (gray) and noise-exposed mice + retigabine (red) after noise exposure and injection for high-frequency (20–32 kHz) sound stimulation (n = 5–20, no statistical difference was observed between retigabine- and saline-injected mice). See end of the manuscript for detailed values for **B**–**D**. Asterisk, p < 0.05. Error bars indicate SEM.

DOI: 10.7554/eLife.07242.010

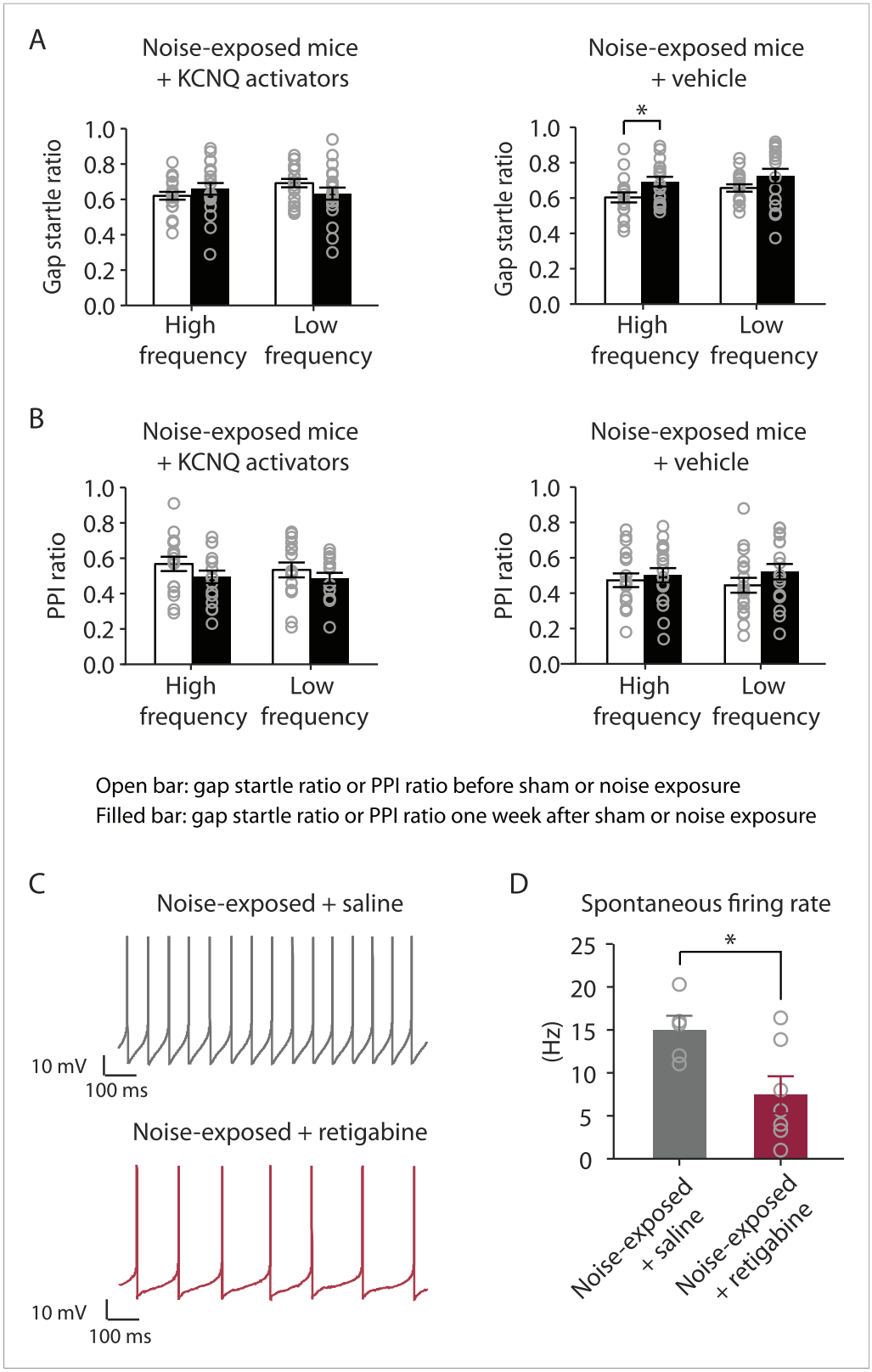


**Figure 7—figure supplement 1**. In vivo administration of KCNQ channel activators prevents the development of tinnitus and reduces the spontaneous firing rate of fusiform cells. **A**. Gap startle ratio of noise-exposed mice with

*Figure 7—figure supplement 1. continued on next page*

*Figure 7—figure supplement 1. Continued*

KCNQ channel activator injection (high frequency background sound: before, 0.62 ± 0.02, after, 0.68 ± 0.02, n = 20, p = 0.06; low frequency background sound: before, 0.70 ± 0.02, after, 0.63 ± 0.03, n = 20, p = 0.06) and with vehicle injection (high frequency background sound: before, 0.61 ± 0.02, after, 0.70 ± 0.03, n = 18, p = 0.01; low frequency background sound: before, 0.66 ± 0.02, after, 0.72 ± 0.03, n = 18, p = 0.08). **B**. PPI ratio of noise-exposed mice with KCNQ channel activator injection (high frequency background sound: before, 0.56 ± 0.03, after, 0.49 ± 0.03, n = 20, p = 0.12; low frequency background sound: before, 0.54 ± 0.03, after, 0.48 ± 0.02, n = 20, p = 0.16) and with vehicle injection (high frequency background sound: before, 0.47 ± 0.03, after, 0.51 ± 0.03, n = 18, p = 0.11; low frequency background sound: before, 0.44 ± 0.04, after, 0.52 ± 0.03, n = 18, p = 0.36). **C**. Representative spontaneous action potentials of fusiform cells from noise-exposed mice injected with either saline (Upper trace, gray) or retigabine (Lower trace, red) twice a day for 6 days. **D**. Summary graph showing spontaneous firing rate of fusiform cells from noise-exposed mice injected with either saline or retigabine twice a day for 6 days (noise-exposed mice with saline: 15.0 ± 1.5 Hz, n = 5; noise-exposed mice with activator: 7.5 ± 2.2 Hz, n = 7, p = 0.02). Whole-cell voltage-follower mode recordings (current clamp, at I = 0) were performed 7 days after noise exposure and in the presence of excitatory and inhibitory receptor antagonists (20 μM DNQX, 20 μM SR95531, and 0.5 μM strychnine). Asterisk, p < 0.05. Error bars indicate SEM.

DOI: 10.7554/eLife.07242.011

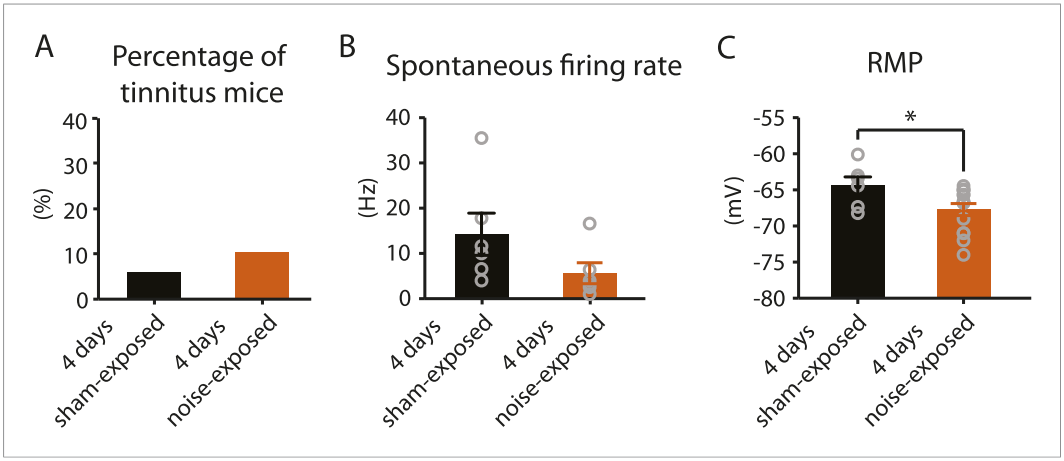


**Figure 8**. 4 days after noise exposure, mice have reduced KCNQ2/3 current amplitude but do not show either hyperactivity or tinnitus. **A**. Percentage of mice that develop tinnitus in 4 days sham-exposed and 4 days noise-exposed mice (4 days sham-exposed: n = 19; 4 days noise-exposed: n = 20, p = 0.28). **B**. Summary graph showing spontaneous firing rate in fusiform cells, assessed with whole-cell, voltage-follower mode recordings (current clamp, at I = 0), from 4 days sham-exposed and 4 days noise-exposed mice (4 days sham-exposed: 14.3 ± 4.7 Hz, n = 6; 4 days noise-exposed: 5.6 ± 2.3 Hz, n = 6, p = 0.13). **C**. Summary graph showing resting membrane potential (RMP) in 4 days sham-exposed mice and 4 days noise-exposed mice (4 days sham-exposed: −64.4 ± 1.2 mV, n = 6; 4 days noise-exposed: −67.7 ± 0.8 mV, n = 14, p = 0.04). Asterisk, p < 0.05. Error bars indicate SEM.

DOI: 10.7554/eLife.07242.012

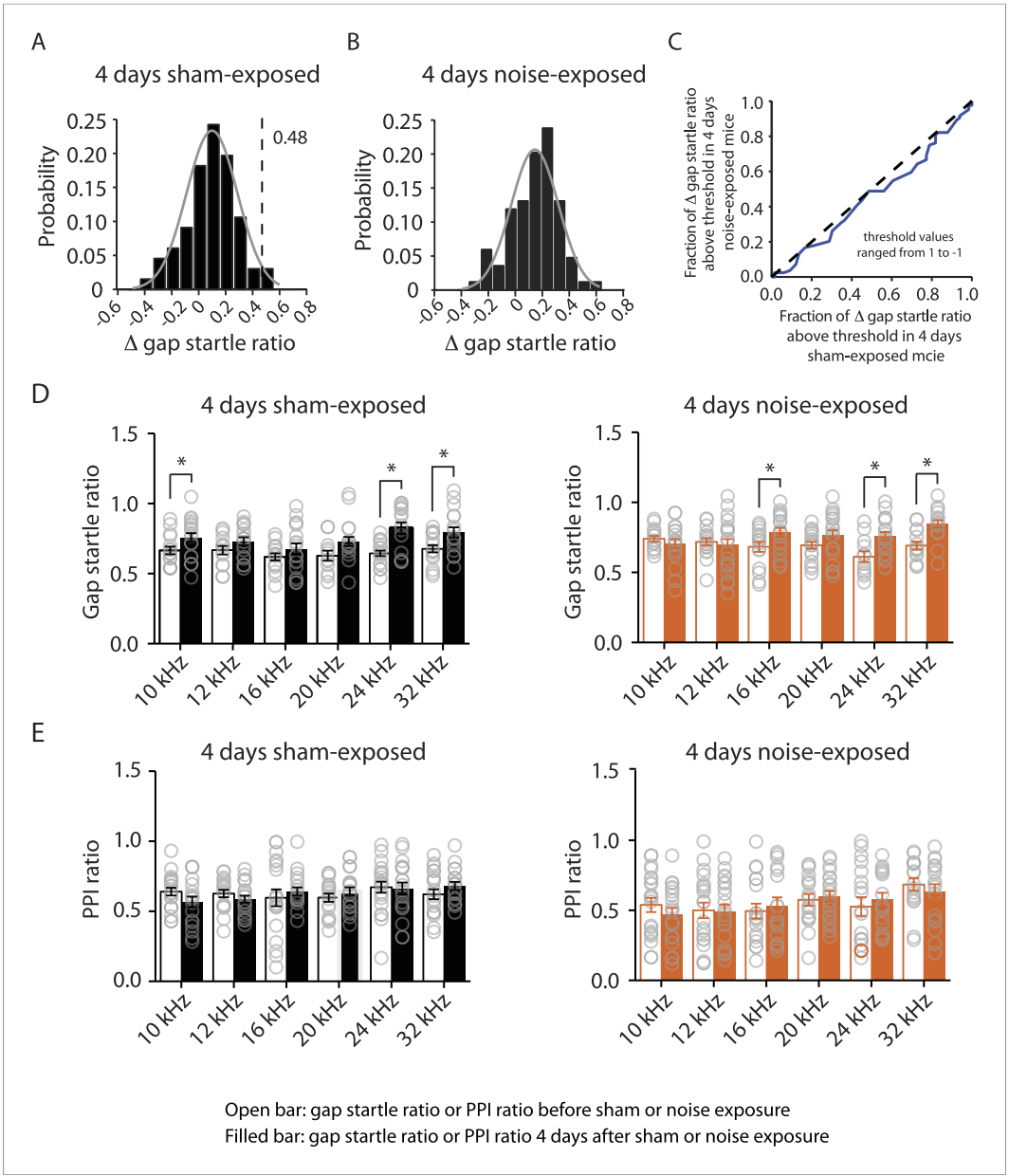


**Figure 8—figure supplement 1**. 4 days noise-exposed mice exhibit similar gap detection and PPI compared to 4 days sham-exposed mice. **A**. Probability distribution of changes in gap startle ratio (Δ gap startle ratio) before and 4 days after sham exposure. The distribution of Δ gap startle ratio represents the changes in gap startle ratios in control (sham-exposed) mice between postnatal P20 - P23 and P24 - P27. Data were fitted by a normal distribution (gray curve, $\mu = 0.09$, $\delta = 0.18$, n = 15). Δ gap startle ratios smaller than 0.48 (dotted line, which is the point that is 2 standard deviations above the mean and used as the threshold for evaluating tinnitus) represent 98.5% of the experimental population and 98.5% of the fitted distribution. **B**. Probability distribution of Δ gap startle ratio before and 4 days after noise exposure. Data were fitted by a normal distribution (gray curve, $\mu = 0.07$, $\delta = 0.12$, n = 15). **C**. Comparison of Δ gap startle ratio distribution between 4 days sham-exposed and 4 days noise-exposed mice shown in A and B for different thresholds. With the threshold ranging from 1 to −1 in 0.02 increments, the fraction of Δ gap startle ratios above threshold in 4 days noise-exposed mice was plotted against the fraction of Δ gap startle ratios above threshold in 4 days sham-exposed mice. Because this relationship was not different from the diagonal line (dotted line), we concluded that the fractions of Δ gap startle ratios above threshold in 4 days noise-exposed mice and 4 days sham-exposed mice were not different. **D**. Summary graph of gap startle ratio for different frequencies of background sound for 4 days sham-exposed mice (10 kHz, before: 0.67 ± 0.03, n = 16, after: 0.78 ± 0.03, n = 20, p =

*Figure 8—figure supplement 1. continued on next page*

*Figure 8—figure supplement 1. Continued*

0.05; 12 kHz, before: 0.67 ± 0.03, n = 14, after: 0.73 ± 0.03, n = 18, p = 0.14; 16 kHz, before: 0.62 ± 0.02, n = 16, after: 0.68 ± 0.04, n = 18, p = 0.27; 20 kHz, before: 0.63 ± 0.04, n = 12, after: 0.73 ± 0.03, n = 19,p = 0.051; 24 kHz, before: 0.64 ± 0.02, n = 19, after: 0.82 ± 0.04, n = 16, p < 0.001; 32 kHz, before: 0.68 ± 0.03, n = 17, after: 0.79 ± 0.04, n = 18, p = 0.01) and 4 days noise-exposed mice (10 kHz, before: 0.74 ± 0.02, n = 15, after: 0.70 ± 0.03, n = 20, p = 0.42; 12 kHz, before: 0.72 ± 0.03, n = 17, after: 0.70 ± 0.04, n = 21, p = 0.68; 16 kHz, before: 0.68 ± 0.04, n = 16, after: 0.79 ± 0.03, n = 19, p = 0.04; 20 kHz, before: 0.69 ± 0.02, n = 18, after: 0.77 ± 0.04, n = 21, p = 0.12; 24 kHz, before: 0.61 ± 0.04, n = 12, after: 0.76 ± 0.03, n = 19, p = 0.005; 32 kHz, before: 0.69 ± 0.03, n = 15, after: 0.85 ± 0.03, n = 18, p < 0.001). **E.** Summary graph of PPI ratio for different frequencies of background sound for 4 days sham-exposed mice (10 kHz, before: 0.62 ± 0.03, n = 21, after: 0.57 ± 0.04, n = 19, p = 0.13; 12 kHz, before: 0.63 ± 0.03, n = 19, after: 0.59 ± 0.03, n = 21, p = 0.28; 16 kHz, before: 0.60 ± 0.06, n = 20, after: 0.64 ± 0.03, n = 19, p = 0.51; 20 kHz, before: 0.60 ± 0.03, n = 19, after: 0.64 ± 0.03, n = 21, p = 0.29; 24 kHz, before: 0.67 ± 0.04, n = 21, after: 0.66 ± 0.04, n = 20, p = 0.87; 32 kHz, before: 0.762 ± 0.04, n = 20, after: 0.68 ± 0.03, n = 18, p = 0.21) and 4 days noise-exposed mice (10 kHz, before: 0.54 ± 0.05, n = 21, after: 0.47 ± 0.04, n = 21, p = 0.33; 12 kHz, before: 0.50 ± 0.06, n = 21, after: 0.49 ± 0.05, n = 21, p = 0.91; 16 kHz, before: 0.50 ± 0.05, n = 19, after: 0.53 ± 0.06, n = 17, p = 0.65; 20 kHz, before: 0.58 ± 0.04, n = 19, after: 0.60 ± 0.04, n = 21, p = 0.63; 24 kHz, before: 0.53 ± 0.07, n = 18, after: 0.58 ± 0.05, n = 18, p = 0.55; 32 kHz, before: 0.68 ± 0.05, n = 17, after: 0.63 ± 0.06, n = 17, p = 0.46). Asterisk, p < 0.05. Error bars indicate SEM. 35 dB, noise-exposed + saline, 815.2 ± 68.3 nV, n = 15, noise-exposed + retigabine, 826.1 ± 76.8 nV, n = 14, p = 0.92; 40 dB, noise-exposed mice + saline, 947.8 ± 81.0 nV, n = 16, noise-exposed + retigabine, 1054.5 ± 104.8 nV, n = 14, p = 0.42; 45 dB, noise-exposed + saline, 963. 2 ± 69.9 nV, n = 14, noise-exposed + retigabine, 1163.5 ± 129.1 nV, n = 13, p = 0.16; 50 dB, noise-exposed + saline, 1022.6 ± 64.3 nV, n = 16, noise-exposed + retigabine, 1207.6 ± 99.9 nV, n = 14, p = 0.12; 55 dB, noise-exposed + saline, 1247.1 ± 76.7 nV, n = 13, noise-exposed + retigabine, 1266.6 ± 134.5 nV, n = 12, p = 0.90; 60 dB, 1168.4 ± 74.8 nV, n = 9, noise-exposed + retigabine, 1392.2 ± 170.8 nV, n = 10, p = 0.26; 65 dB, noise-exposed + saline, 1097.1 ± 117.0 dB, n = 5, noise-exposed + retigabine, 1183.3 ± 156.0 nV, n = 5, p = 0.67).

DOI: 10.7554/eLife.07242.013

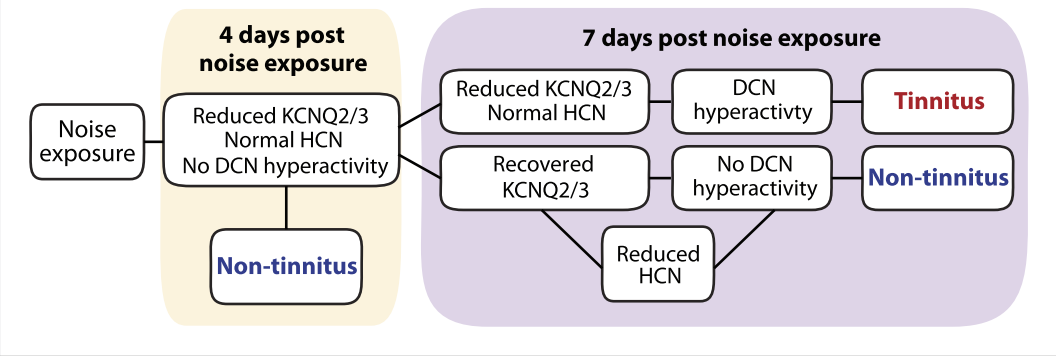


**Figure 9**. Biophysical mechanisms underlying the development of vulnerability and resilience to noise-induced tinnitus. Diagram illustrating the noise-induced plasticity of KCNQ2/3 and HCN channel activity, the emergence of DCN hyperactivity, and the development of vulnerability and resilience to tinnitus.

DOI: 10.7554/eLife.07242.014